Proteomic Characteristics of the Giant Congenital Melanocytic Nevi

Yong Kyu Kim

Department of Medicine

The Graduate School, Yonsei University

Proteomic Characteristics of the Giant Congenital Melanocytic Nevi

Directed by Professor Kwan-Chul Tark

Doctoral Dissertation
Submitted to the Department of Medicine

the Graduate School of Yonsei University
in partial fulfillment of the requirements for the degree
of Doctor of Philosophy

Yong Kyu Kim

This certifies that the Doctoral Dissertation of Yong Kyu Kim is approved.

Thesis Supervisor: Kwan Chul Tark

[Kwang Hoon Lee: Thesis Committee)

[Kap Sung Oh: Thesis Committee)

[Hoguen Kim: Thesis Committee)

[Dae Hyun Lew: Thesis Committee)

The Graduate School
Yonsei University

ACKNOWLEDGEMENTS

I am heartily thankful to my supervisor, Professor Kwan Chul, Tark whose encouragement, guidance and support from the initial to the final level enabled me to develop an understanding of the subject. Also I specially thank to Professor Kwang Hoon Lee, Kap Sung Oh, Hoguen Kim, and Dae Hyun Lew.

I would like to thank to my brother, he advised me whenever I faced difficulties

Lastly, I offer my regards and blessings to all of my family who supported me in any respect during the completion of the project.

Yong Kyu Kim

<TABLE OF CONTENTS>

LIST OF FIGURES

LIST OF TABLES

ABSTRACT

Proteomic Characteristics of the Giant Congenital Melanocytic Nevi

Yong Kyu Kim

Department of Medicine
The Graduate School, Yonsei University

(Directed by Professor Kwan Chul Tark)

Background: Giant congenital melanocytic nevi (GCMN) are distress to patients and parents for two reasons. One is disfigurement and the other is possibility of malignant change. But development of GCMN and the underlying mechanism of melanotumorigenesis in GCMN are unknown.

Objective: The aim of this study was to identify the proteomic alterations and associated functional pathways in GCMN.

Methods: We harvested 6 GCMN skins and 6 normal skins which were harvested from 3 GCMN donor patient and 3 from normal patient who were treated in plastic surgery department. Mean age of patient is 8.9 years. Group 1 samples include 3 GCMN and 3 normal skin samples(2 matched skins and 1 normal skin) which were used for proteomic analysis with One dimensional liquid chromatography mass spectrometry(1D-LC MS/MS) analysis and Group 2 samples include 3 GCMN and 3 normal skin samples(2 normal skins and 1 matched skin) were used for western blotting analysis.

The properties of the differentially expressed proteins (DEPs) were then

further analyzed using the bioinformatics tools STRING, PANTHER, and ClueGO.

Results: Among the total proteins in GCMN, changes in the expression of 50 were found to be DEPs significantly ($p < 0.05$, student t-test) down (4 proteins) or upregulated (46 proteins). Among the DEPs with a molecular function, chaperone proteins (15.7% of total DEPs) were the most highly altered, whereas among the DEPs involved in biological processes, alterations were mostly seen in signal transduction proteins (15.3% of total DEPs). Specifically, neurotrophin signaling, melanosome, and downregulated of MTA-3 in ER-negative breast tumors proteins were maximally implicated. Moreover, increases in the expression of members of the 14-3-3 protein family appeared be associated with key cellular biological functions in GCMN. Among the five isoforms of the 14-3-3 family (alpha, beta, zeta, epsilon, and tau), western blot analysis confirmed the upregulation of 14-3-3 epsilon in GCMN.

Conclusion: We found the intensive alteration of 14-3-3 family proteins as a possible key regulator of GCMN biological pathway remodeling, which has important role in development of GCMN and could be associated with melanotumorigenesis.

Key Words: congenital melanocytic nevi, melanotumorigenesis, melanoma, 14-3-3 epsilon.

Proteomic Characteristics of the Giant Congenital Melanocytic Nevi

Yong Kyu Kim

Department of Medicine
The Graduate School, Yonsei University

(Directed by Professor Kwan Chul Tark)

I. Introduction

Giant congenital melanocytic nevi (GCMN) are pigment cell malformations that are visible at birth, as well as nevi manifesting congenital features that become clinically apparent shortly after birth [1]. In either case, they are likely the result of aberrant melanocyte migration, differentiation, and deposition in the dermis during the early stages of embryogenesis [2].

Although the absolute risk for developing melanoma in association with GCMN is low, GCMN is considered to be a risk factor in malignant melanoma [3], especially in individuals with larger malformations (over 20 cm in diameter) [4]. Several genomic and proteomic analysis have been performed to elucidate the mechanism of melanotumorigenesis from GCMN. Gene-based analyses revealed that oncogenic *BRAF* [5] and *NRAS*

[6] mutations are frequently seen in GCMN. Also, broad Bcl-2 expression in GCMN has been suggested to suppress apoptosis, which otherwise plays an important role in the maintenance of nevocytes [7]. In spite of these observations, the major biological processes and pathways of melanotumorigenesis remain unclear.

Proteomic profiling of certain diseases has been increasingly used to acquire data on a large number of proteins to identify potential biomarkers and to gain insight into the underlying mechanisms of a variety of diseases. However, the massive amount of generated information often only increases the complexity of these analyses. In response, a systemic approach to the proteomic data was developed. In this study, the systemic properties of GCMN were assessed, with the aim of gaining insight into the functional association between GCMN and melanotumorigenesis. Specifically, we used label-free liquid chromatography-mass spectrometry (LC-MS) proteomics and applied bioinformatics tools to identify proteins that may play a key role in the malignant transformation of GCMN. A total of 50 proteins (DEPs) found to be differentially expressed in normal skin and GCMN could be tightly organized in functional clusters. Importantly, several members of the 14-3-3 family of proteins, thought to be regulators of oncogenesis, were

found to be upregulated. The results of this study might improve our understanding of the possible mechanisms that give rise to GCMN melanotumorigenesis.

II. Materials and Methods

1. Patients

3 normal skin samples and 6 GCMN samples from GCMN patients were obtained and 3 normal skin samples were obtained from patients who underwent scar revision or skin graft procedures in the Department of Plastic Surgery, Inje University Ilsan Paik Hospital, Korea. The collection and use of the samples were approved by the institutional review board of Inje University Ilsan Paik Hospital.

2. Sample preparation

All skin samples were defatted surgically. Excised skin samples were categorized as 2 groups for analysis and validation, Group 1 include 3 GCMN and 3 normal skin samples (2 matched skins and 1 normal skin) for proteomic analysis with 1D-LC MS/MS analysis. Group 2 include 3 GCMN and 3 normal skin samples (1 matched skin and 2 normal skins) for western blotting analysis.

Group 1 samples were ground to a powder in liquid nitrogen, dissolved in lysis buffer (9 M urea, 2 M thiourea, 4% CHAPS (3-[(3-cholamidopropyl)dimethylammonio] -1-propanesulfonate), 40 mM dithiothreitol, and 1% protease inhibitor cocktail), vortexed, and

incubated on ice for 1 h. The mixture was then centrifuged (10,000 × *g*, 30 min, 4°C) and the total proteins contained in the supernatant used for the experiments. The total protein content of the solution was determined using the 2D Quant kit (GE Healthcare, Milwaukee, WI, USA), with serum BSA (0–50 mg/mL) as the standard.

3. One-dimensional LC-ESI-MS/MS proteome analysis

Protein separation and LC-MS analysis were performed as previously described [8]. Briefly, dissolved skin proteins were separated on a 12% polyacrylamide gel by SDS-PAGE. The gels were washed three times with ddH_2O for 5 min each and then stained with Bio-Safe Coomassie stain solution (Coomassie G250 stain; Bio-Rad, Hercules, CA, USA) for 1 h, with gentle shaking at room temperature. The 15 protein bands detected on the Coomassie-stained gels were evenly excised and then destained by incubation in 75 mM ammonium bicarbonate/40% ethanol (1:1). Disulfides were reduced by treatment with 5 mM DTT/25 mM ammonium bicarbonate at 60°C for 30 min, followed by alkylation with 55 mM iodoacetoamide at room temperature for 30 min. The gel pieces were then dehydrated in 100% acetonitrile (ACN), dried, and swollen overnight at 37°C in 10 µl 25 mM ammonium bicarbonate buffer

containing 20 μg modified sequencing grade trypsin (Roche Applied Science, Indianapolis, IN, USA)/ml. The tryptic peptide mixture was eluted from the gel with 0.1% formic acid. LC-MS/MS analysis was performed using a ThermoFinnigan ProteomeX workstation LTQ linear ion trap MS (Thermo Electron, San Jose, CA, USA) equipped with NSI sources (Thermo Electron). Briefly, 12 μl of peptide sample from the in-gel digestion was injected and loaded onto a peptide trap cartridge (Agilent, Palo Alto, CA, USA). Trapped peptides were eluted onto a 10cm reversed-phase (RP) PicoFrit column packed in-house with 5μm 300-Å pore size C18, then separated by gradient elution. The mobile phases consisted of H_2O and ACN, both containing 0.1% v/v formic acid. The flow rate was maintained at 200 nl/min. The gradient started at 2% ACN, then reached 60% ACN in 50 min, 80% ACN in the next 5 min, and 100% H_2O in the final 15 min. Data-dependent acquisition (*m/z* 400–1800) was enabled, and each MS survey scan was followed by five MS/MS scans within 30 s, with the dynamic exclusion option enabled. The spray voltage was 1.9 kV, the temperature of the ion transfer tube 195°C, and the normalized collision energy was 35% [8].

Data-analyzed tandem mass spectra were extracted and the charge state deconvoluted and de-isotoped using the Sorcerer 3.4 beta 2 platform

(Sorcerer software 3.1.4, Sorcerer Web interface 2.2.0 r334, and Trans-, Proteomic Pipeline 2.9.5). All MS/MS samples were analyzed using SEQUEST (version v.27, rev. 11; ThermoFinnigan, San Jose, CA, USA), which was set to search the ipi 3.29 database (IPI ver.3.29, 40131 entries) with semitrypsin as the digestion enzyme. The search used a fragment-ion mass tolerance of 1.00 Da and a parent-ion mass tolerance of 1.5 Da. Iodoacetamide-derivatized cysteine was specified as a fixed modification. Methionine oxidation, iodoacetamide derivatizion of cysteine, and phosphorylation of serine, threonine, and tyrosine were specified as variable modifications.

4. Validation of MS/MS identification and label free quantification

Scaffold (version Scaffold-2.0; Proteome Software Inc., Portland, OR) was used to validate MS/MS-based peptide and protein identifications. Peptide identifications were accepted if their probability was >95.0%, as specified by the Peptide Prophet algorithm, and they contained at least one identified peptide. Protein probabilities were assigned by the Protein Prophet algorithm. Proteins containing similar peptides such that they could not be differentiated based on MS/MS analysis alone were grouped to satisfy the principles of parsimony. The peptide false positive (FPR)

rate was calculated using the Scaffold software. For each charge state, incorrect assignments were tabulated to calculate the FPRi = [(#Assigned Incorrect at 95% probability)/(Total# Incorrect Assigned)]*100, with *i* being the charge state. The assignment is considered correct if it is associated with a protein that has a 95% probability, according to the Protein Prophet algorithm, and if a minimum of 2 peptides are matched with the protein sequence, each with a 95% probability, based on the Peptide Prophet algorithm. After identifying the proteins, each dataset was used for a subtractive analysis by quantitative value. Quantitative value of proteome set was analyzed by label free mass spectrometry which count each spectra peaks and normalizes in the Scaffold program[9].

5. Bioinformatics analysis

Systematic bioinformatics analysis of the GCMN proteome was conducted using STRING 8.3 (Search Tool for the Retrieval of Interacting Genes/Proteins) [10], PANTHER 7.0 (Protein Analysis Through Evolutionary Relationships) classification system [11], the NCBI Clusters of Orthologous Groups (COG) database [12], Cytoscape, and ClueGO [13].

6. Western blot analysis

Selected 14-3-3 family proteins were analyzed by Western blot to confirm the proteomic results. The proteins were prepared as follows: normal skin and GCMN (n = 3 each) were homogenized in lysis buffer (Tris–HCL 20 mM, NaCl 150 mM, EDTA 10 mM, NaF 50 mM, $NaVO_4$ 25 mM) and centrifuged at 15,000 × *g* for 10 min. Equal amounts of membrane proteins (30 μg) were separated by 8% SDS-PAGE, followed by electrophoretic transfer of the proteins to nitrocellulose membranes and blocking overnight in 5% skim milk. The blocked membrane was incubated with primary antibodies against 14-3-3 alpha+beta (30 kDa), 14-3-3 epsilon (29 kDa), 14-3-3 zeta (28 kDa), 14-3-3 sigma (25 kDa), 14-3-3 tau (31 kDa), or β-tubulin (55 kDa) (Abcam, Cambridge, MA) for 2 h at room temperature. The membranes were then washed three times with PBS and incubated with secondary antibodies [goat anti-mouse IgG (Abcam) against 14-3-3 sigma, 14-3-3 theta, and β-tubulin; goat anti-rabbit IgG (Abcam) against 14-3-3 alpha+beta, 14-3-3 epsilon, 14-3-3zeta] for 2 h at room temperature. Images were captured and quantified using a Fuji Imager LAS3000 (FujiFilm, Miyagi, Japan) at 75% of total resolution and 10 to 60s exposure time using the Multi-Gauge V2.3 system.

7. Statistical analysis

Student's t-test was used to compare the characteristics of the donors and samples of normal skin and GCMN. $P < 0.05$ was considered statistically significant.

III. Results

1. Characteristics of the study population

The average age of the patients contributing the normal skin and GCMN samples was not significantly different (10.5 ± 5.31 and 6 ± 1.89, respectively, $p = 0.09$). All GCMN were over 15 cm in diameter. Three of the six normal skin samples taken from GCMN donors were analyzed using LC-MS or western blotting to minimize environmental bias between individuals (Table 1).

Table 1. Clinical characteristics of GCMN and normal skin samples

Sample ID	Age	Sex	Location	Surgery
Group 1				
Normal 1*	8	Male	Groin	Skin graft
Normal 2*	5	Female	Face	Scar revision
Normal 3	14	Female	Face	Scar revision
GCMN 1*	8	Male	Face	
GCMN 2*	5	Female	Face	
GCMN 3	8	Male	Forehead	
Group 2				
Normal 4*	6	Female	Groin	Skin graft
Normal 5	11	Female	Face	Scar revision
Normal 6	19	Female	Face	Scar revision
GCMN 4*	6	Female	Face	
GCMN 5	6	Female	Abdomen	
GCMN 6	3	Female	Left leg	

* matched skin sample

2. Proteomic alterations in GCMN

The same amount (20 μg) of soluble proteins was separated using SDS-PAGE, which resulted in 15 bands (Figure 1A). The peptide spectrum peak of each protein band was acquired (Supplementary Figure S1), thereby identifying 438 nonredundant proteins. Among these, 343 proteins were commonly identified in both groups, 62 were detected only in GCMN, and 33 only in normal skin (Figure 1B). Fifty differentially expressed proteins (DEPs) were identified, i.e., their expression was significantly ($p < 0.05$) different in GCMN than in normal skin (Figure 1C). The large majority of these DEPs were upregulated (46 of 50, 92%) and very few (4 proteins, 8%) were downregulated (Figure 2, Supplementary Table S1). The most highly upregulated protein in GCMN was cathepsin D (CTSD), which was expressed at a 6.8-fold higher level than in normal skin. In addition, protein disulfide-isomerase A3 precursor (PDIA3, 5.4-fold), prohibitin (PHB, 5.3-fold), heat shock protein 70 (HSPA8, 5.2-fold), D-3-phosphoglycerate dehydrogenase (PHGDH, 5-fold), and ATP synthase subunit beta (ATP5B, 5-fold) were highly (>4-fold) upregulated in GCMN. The four proteins downregulated in GCMN were cytokeratin-1 (KRT1, –1.4-fold), filaggrin 2 (FLG2, –4.7-fold), hornerin (HRNR, 6.0-fold), and alcohol dehydrogenase 1B

(ADH1B, 6.2fold). Note that CTSD overexpression was found in breast cancer[14], ovarian cancer [15], and human melanoma [16, 17].

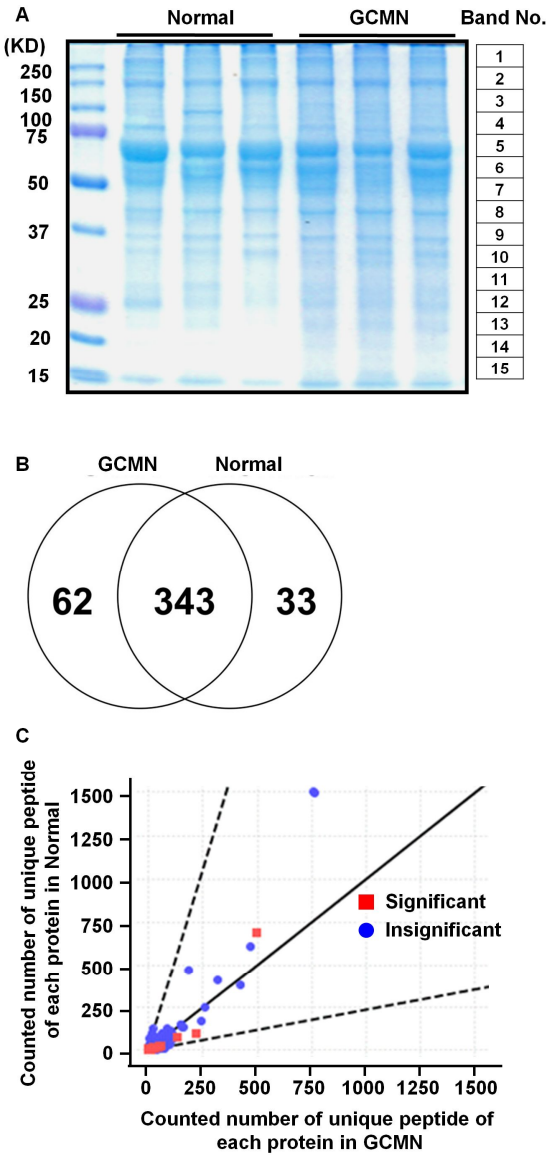

Figure1. Comparative proteomic analysis of giant congenital melanocytic nevi (GCMN) and normal skin using 1D-ESI-LC MS/MS analysis. (A) Coomasie-stained gel of normal skin and GCMN proteins (n = 3 each).

Band number indicates the matching mass peak result in Supplementary Figure S1. (B) Venn diagram of identified proteins in normal and GCMN skin. (D) Statistical test of normal skin vs. GCMN proteomes. The number of unique peptides of each protein in normal skin and GCMN was compared using Student's t-test, with $p < 0.05$ considered to be significant.

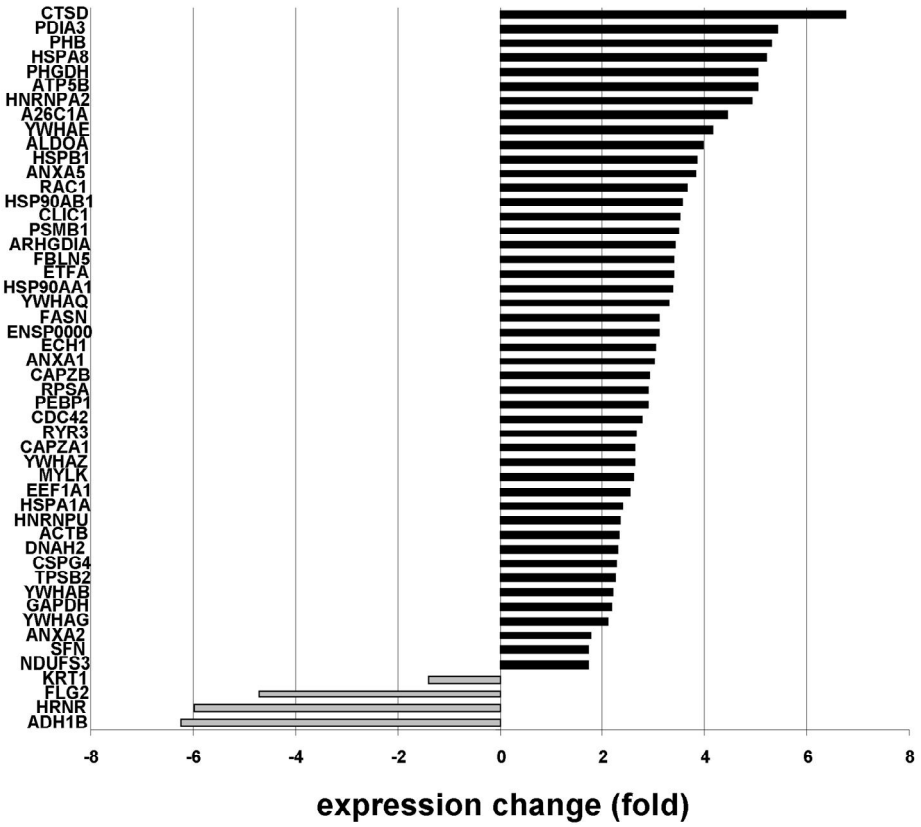

Figure 2. Expressional changes of differentially expressed proteins (DEPs) in GCMN. The histogram displays the protein symbol and the averaged expressional rate of each DEP in GCMN. DEPs comprised 4 downregulated and 46 upregulated proteins in GCMN vs. normal skin.

3. Systemic properties of altered GCMN proteome

The molecular function, biological process association, and COG of 50 DEPs were analyzed to gain insight into the systemic properties of the proteome of GCMN. Among the GCMN proteins with a molecular function, alterations in the expression of chaperones (16% of total), oxidoreductases (8%), and cytoskeletal elements (7%) were determined (Figure 3A). Among the GCMN proteins involved in biological processes, signal transduction (15%), cell structure and motility (10%), protein metabolism and modification (10%), and cell cycle (10%) proteins were markedly altered in their expression. The COG classification showed that the DEPs in GCMN were highly enriched in proteins involved in posttranslational modification, turnover, chaperones (30%), and the cytoskeleton (12%) (Figure 3C), which are consistent with the molecular function and biological process classifications.

Further network analysis with ClueGO was carried out to identify enriched functional groups in GCMN, thus providing detailed information on each one. As ontology sources, GO_biological process, GO_cellular component, GO_molecular function, KEGG pathway, and Reactome_biocarta were selected. The specific functional groups thus identified as significantly enriched in GCMN were melanosome

(GO_cellular component), neurotrophin signaling pathway (KEGG pathway), downregulated of MTA-3 in ER-negative breast tumors (Biocarta), cell cycle (KEGG pathway), phospholipase inhibitor activity (GO_molecular function), and glycolysis/gluconeogenesis (KEGG pathway) (Table 2, Supplementary Figure S2).

Since proteins rarely act alone but rather interact as a group, thus comprising a functional cluster, a protein–protein interacting network was constructed using STRING 8.0. This network consisted of 49 of the 50 DEPs, with 71 interactions between them. As seen in Figure 4A, overlaying the expressional alteration rate of GCMN on this network demonstrated the fold-change in GCMN vs. normal skin. In the GCMN network, upregulated proteins were tightly linked with each other, forming a large cluster. The biological meaning of the cluster was determined by overlaying the COG of each protein on the network, which revealed that closely neighboring proteins shared COGs (Figure 4B). Moreover, the GCMN network contained a very highly specific protein cluster, identified as the 14-3-3 protein family, whose members were expressed at significantly higher levels than in normal skin: 14-3-3sigma (or SFN, 1.7-fold), 14-3-3 protein beta/alpha (YWHAB, 2.2-fold), 14-3-3 protein epsilon (YWHAE, 4.2-fold), 14-3-3 protein

gamma (YWHAG, 2.1fold), 14-3-3 protein theta (YWHAQ, 3.3fold), and 14-3-3 protein zeta/delta (YWHAZ, 2.6fold).

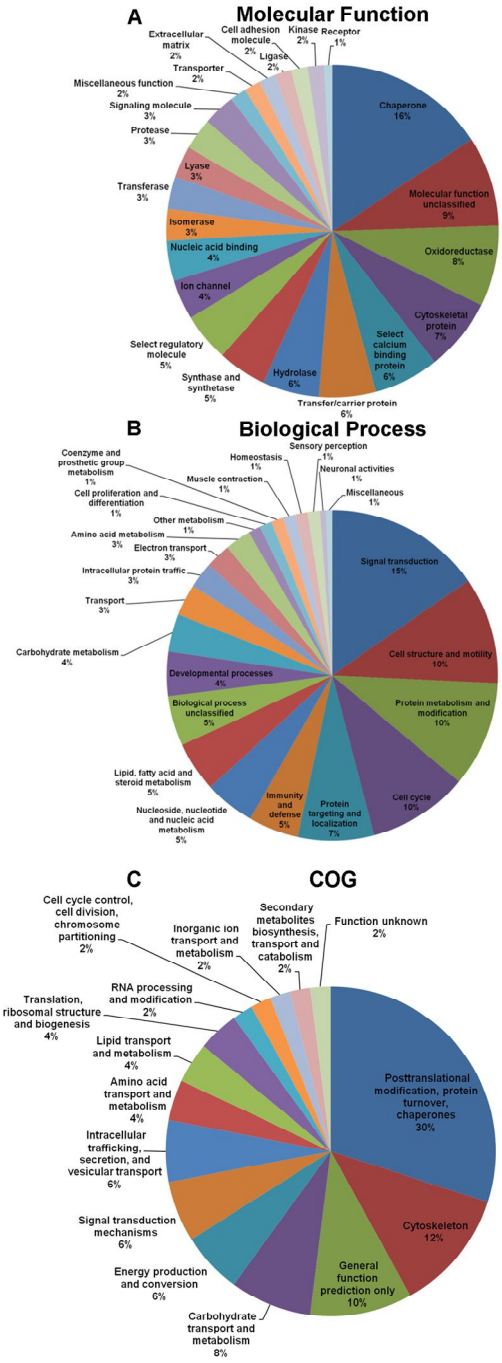

Figure 3. Functional categories and the corresponding percentages in the

GCMN proteome. Molecular function (A), biological process (B), and clusters of orthologous groups (COG) (C) were analyzed using the online bioinformatics analysis tools PANTHER (http://www.pantherdb.org/) and COGnitor provided by the NCBI database (http://www.ncbi.nlm.nih.gov/COG/old/xognitor.html).

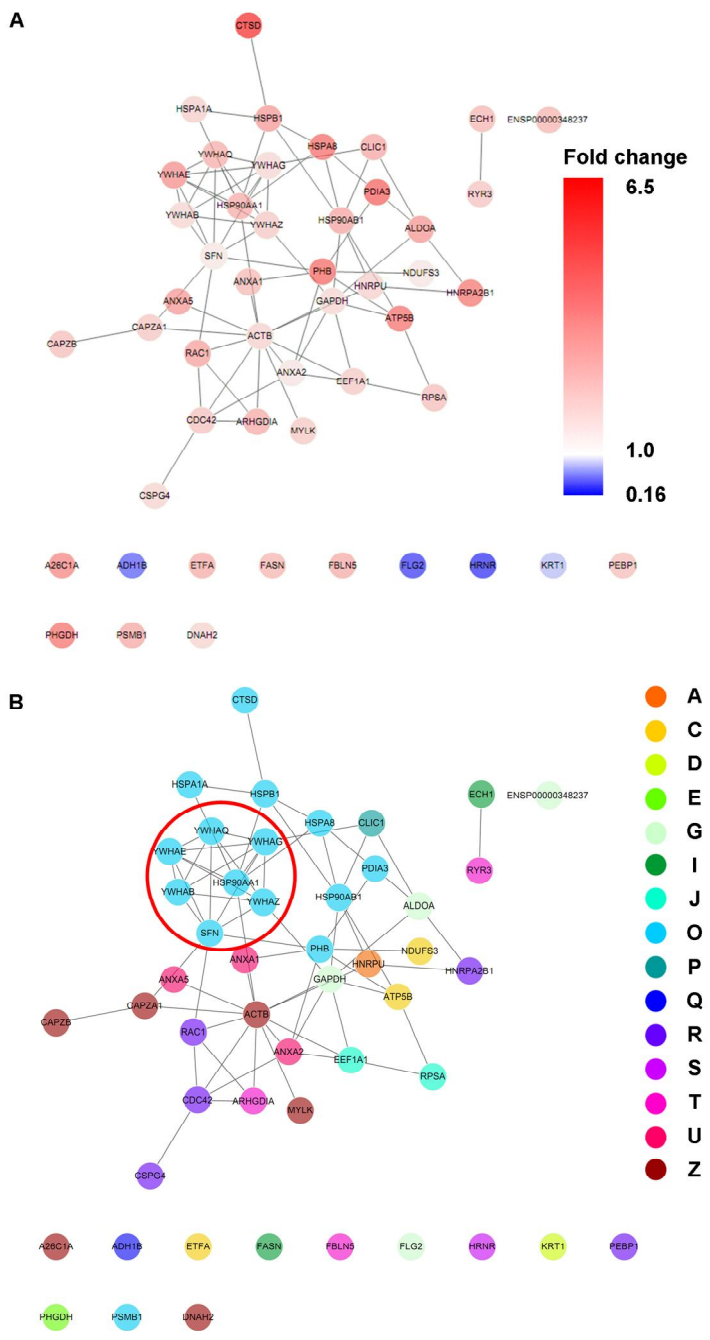

Figure 4. The proteome network of congenital melanocytic nevi. (A)

Protein–protein interactions between proteins in GCMN, as analyzed by String 8.0 and visualized with respect to expression of the corresponding protein. (B) The network overlapped with COG functional clustering. The proteins 14-3-3sigma (or SFN, 1.7-fold), 14-3-3beta/alpha (YWHAB, 2.2-fold), 14-3-3 epsilon (YWHAE, 4.2-fold), 14-3-3gamma (YWHAG, 2.1-fold), 14-3-3theta (YWHAQ, 3.3-fold), and 14-3-3zeta/delta (YWHAZ, 2.6-fold) were tightly linked with each other and formed specific functional clusters (red circles). A: RNA processing and modification, C: Energy production and conversion, D: Cell cycle control, cell division, chromosome partitioning, E: Amino acid transport and metabolism, G: Carbohydrate transport and metabolism, I: Lipid transport and metabolism, J: Translation, ribosomal structure, and biogenesis, O: Posttranslational modification, protein turnover, chaperones, P: Inorganic ion transport and metabolism, Q: Secondary metabolites biosynthesis, transport, and catabolism, R: General function prediction only, S: Function unknown, T: Signal transduction mechanisms, U: Intracellular trafficking, secretion, and vesicular transport, Z: Cytoskeleton.

Table 2. Altered major biological pathways in GCMN

GOID	% Genes[1]	p-Value[2]	p-Value/ Bonf[3]	Involved Proteins
Cell cycle				
KEGG:04110	5	9.0E-07	4.77E-05	ANXA1|SFN|YWHAB|YWHAE|YWHAG| YWHAQ|YWHAZ
Phospholipase inhibitor activity				
GO:0004859	27.3	3.2E-06	1.68E-04	ANXA1|ANXA2|ANXA5|ARHGDIA|ATP5 B|KRT1
Melanosome				
GO:004247	12.8	4.1E-16	2.17E-14	ANXA1|ANXA2|ANXA5|ATP5B|CLIC1|C TSD|FASN|HRNR|HSP90AA1|HSP90AB1| HSPA1B|HSPA8|HSPB1|KRT1|PDIA3|RA C1|SFN|YWHAB|YWHAE|YWHAG|YWH AZ
Neurotrophin signaling pathway				
KEGG:04722	6.1	2.4E-09	1.25E-07	ACTB|ARHGDIA|CAPZA1|CAPZB|CDC42 |HSPB1|MYLK|RAC1|SFN|YWHAB|YWH AE|YWHAG|YWHAQ|YWHAZ
Downregulated of MTA-3 in ER-negative breast tumors				
BioCarta:204	28.6	4.9E-08	2.62E-06	ADH1B|ALDOA|CTSD|ECH1|GAPDH|HSP B1|PHGDH|RYR3
Glycolysis/Gluconeogenesis				
KEGG:00010	4.7	7.2E-04	0.038	ADH1B|ALDOA|ECH1|FASN|GAPDH

[1]% of associated genes identified in our results/total known genes involved in the function or pathway, [2]Term p-Value,[3]Term p-Value with Bonferroni correction

4. Western blot analysis of 14-3-3 family proteins

The 14-3-3 family proteins in normal and GCMN skin (n = 3 each) were analyzed by Western blotting using samples distinct from the proteomic specimens. A comparison with normalized β-actin expression showed that the expression of 14-3-3 epsilon was 2.41 ± 0.26 fold ($p < 0.005$) higher in GCMN than in normal skin.

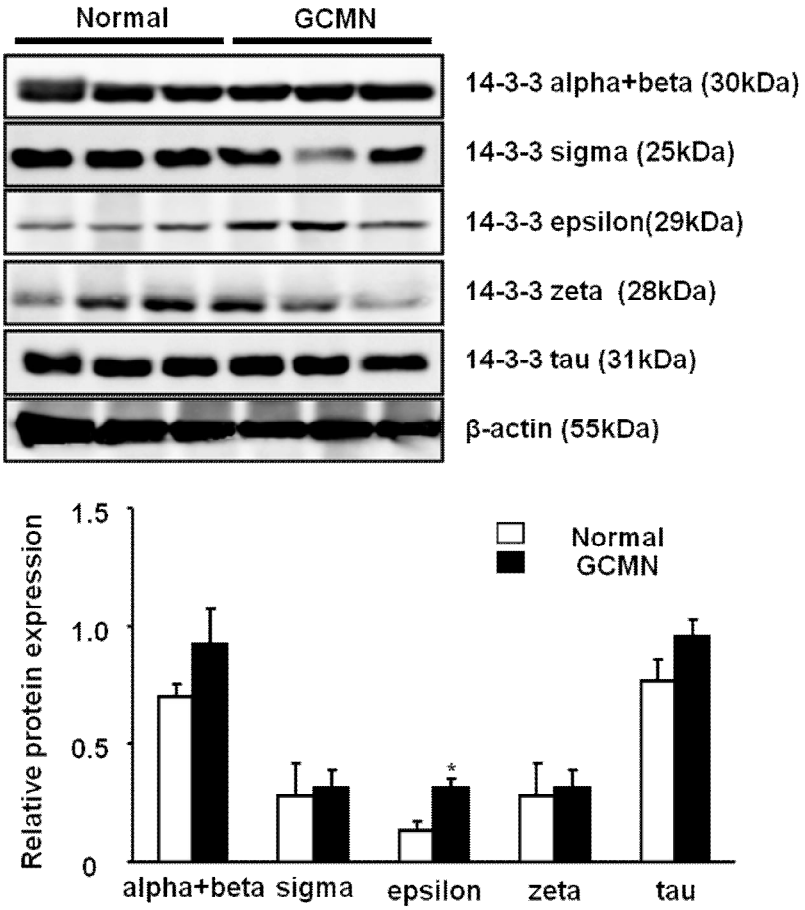

Figure 5. Expressional alterations in the 14-3-3 protein family. Western blotting shows significantly increased 14-3-3 epsilon expression in the GCMN group. *$p < 0.05$, Student's t-test ($n = 3$ in each group)

IV. Discussion

In the present study, the proteomic composition of GCMN was compared with that of normal skin. A major aim of the study was the identification of proteins whose expression is enhanced in GCMN to gain insight into the mechanism of melanotumorigenesis in these malformations. LC-ESI-MS/MS analysis showed that 50 of the 438 identified proteins were differentially expressed between normal skin and GCMN. Among the latter, 92% were upregulated but only 8% were downregulated. The use of different bioinformatics tools showed that GCMN clearly differed from normal skin in terms of protein expression patterns, which suggested that specific biological processes are altered in GCMN. As derived from the GO categories, KEGG pathways, and Reactome_biocarta, these processes were shown to encompass several major biological functions, i.e., the neurotrophin signaling pathway, downregulated of MTA-3 in ER-negative breast tumors, the cell cycle, phospholipase inhibitor activity, and glycolysis/gluconeogenesis. Strikingly, among these, neurotrophin signaling[18, 19], MTA-3 downregulation[20], cell cycle deregulation[21], and glycolysis/gluconeogenesis [22] have been implicated in the development and progression of melanoma and other cancers. This suggests that

proteomic modifications with tumorigenic potential are present in GCMN.

Our results also revealed the highly increased expression of cathepsin D (CTSD), a molecular maker of malignant cancers, in GCMN. CTSD overexpression has also been reported in breast cancer [14], ovarian cancer [15], and human melanoma [16, 17]. In contrast, a comparative proteomic analysis of melanocytes and melanoma showed that CTSD is downregulated in melanoma [23].

The 14-3-3 proteins comprise a highly conserved family whose members are found in both plants and mammals. They mediate signal transduction by binding to phosphoserine-containing proteins and are involved in many biological cellular processes, such as metabolism, protein trafficking, signal transduction, apoptosis, and cell cycle regulation, through interaction with various phosphoserine-containing proteins, such as CDC25 phosphatases, RAF1, and IRS1 proteins. The 14-3-3 family proteins consist of seven isoforms: beta, gamma, epsilon, sigma, zeta, tau, and eta. The alpha and sigma isoforms are the phosphoforms of beta and zeta, respectively. All 14-3-3 proteins are ubiquitously expressed, with the exception of 14-3-3sigma, which is exclusively expressed in epithelial cells [24]. Their properties include self

assembly into homo- and heterodimers and the ability to enhance the activity of many proteins with proliferative and/or survival functions, such as Raf kinases, and to inhibit pro-apoptotic proteins, such as Bad, Bim, and Bax [25-27]. Among the 14-3-3 family members, 14-3-3 sigma acts as a tumor suppressor and its expression is upregulated coordinately with that of p53 and BRCA1[28]. Since DNA damage induces 14-3-3 sigma gene expression, the overexpression of this gene or its respective protein is frequently found in cancers such as ovarian carcinomas [29], pancreatic cancer [30], papillary carcinoma [31], hepatocellular and carcinoma [31]. In addition, high frequency of hypermethylation at the 14-3-3 sigma locuswas implicated with breast cancer [32]. Given that the loss of 14-3-3sigma expression sensitizes tumor cells to treatment with conventional cytostatic drugs, modulation of 14-3-3 sigma activity might be an attractive therapeutic approach [33]. In our proteomic results, expression of 14-3-3 proteins was significantly higher in GCMN than in normal skin, which strongly supports the greater tendency to melanotumorigenesis in GCMN. In particular, the enhanced expression of 14-3-3 epsilon protein was clearly shown in Western blot analysis (Figure 5).

Compared to the other isoforms, little is known about the molecular

and biological role of 14-3-3 epsilon. However, 14-3-3 epsilon has been shown to have an essential role in cell development. Studies in *Drosophila* showed that 14-3-3 epsilon is required for the correct timing of mitosis in undisturbed post-blastoderm cell cycles [34]. More recently, defects in neuronal migration during the development of 14-3-3 epsilon knockout mice were reported [35].

The phosphorylation-induced binding of 14-3-3 epsilon to the pro-apoptotic transcription factor forkhead transcription factor like 1 (FKHRL1 or FOXO3a) leads to structural changes and inhibits the protein's pro-apoptotic activity [36]. In inflammation and carcinogenesis, 14-3-3 epsilon interacts with key molecules of the mitogen-activated protein kinase (MAPK) signal module to selectively modulate tumor necrosis factor-alpha (TNF-α)-induced nuclear factor-kappa-beta (NF-κB) activity [37]. The function and regulatory mechanism of 14-3-3 epsilon in carcinogenesis is controversial and appears to be tumor-specific. Expression of the protein is higher in renal cancerous tissues than in normal kidney [38]. Moreover, based on their involvement in the tumorigenesis of meningioma, 14-3-3 epsilon, zeta, and theta may be efficient markers for predicting the degree of malignancy of these tumors [39]. In contrast, mRNA and protein expression of 14-3-3 epsilon in

laryngeal squamous cell carcinoma tissues was shown to be significantly lower than in normal tissues[40]. An early role in tumorigenesis is suggested by the observation that 14-3-3 epsilon expression is increased in intrinsically aged and photoaged human skin [41].

V. CONCLUSION

Through our study, we found out following things (1) Six important biological process or pathway, including 'melanosome, neurotrophin signaling pathway, downregulated of MTA-3 in ER-negative breast tumors, cell cycle, phospholipase inhibitor activity, and glycolysis/gluconeogenesis, was significantly altered in GCMN skins. (2) The intensive alteration of 14-3-3 family proteins possibly act as central regulator of GCMN biological pathway remodeling, which has important role in development of GCMN and could be associated with melanotumorigenesis.

Because of limitation in available sample, we could not directly check the expression level of 14-3-3 proteins in the tissue of malignant melanoma, thus, we need further study to validate the functional role of 14-3-3 proteins in melanotumorigenesis by comparing malignant melanoma patient with giant congenital melanocytic nevi.

References

1. Rhodes AR, Albert LS, Weinstock MA. Congenital nevomelanocytic nevi: proportionate area expansion during infancy and early childhood. J Am Acad Dermatol 1996;34:51-62.
2. Cramer SF. The melanocytic differentiation pathway in congenital melanocytic nevi: theoretical considerations. Pediatr Pathol 1988;8:253-65.
3. Marghoob AA, Schoenbach SP, Kopf AW, Orlow SJ, Nossa R, Bart RS. Large congenital melanocytic nevi and the risk for the development of malignant melanoma. A prospective study. Arch Dermatol 1996;132:170-5.
4. Krengel S, Hauschild A, Schafer T. Melanoma risk in congenital melanocytic naevi: a systematic review. Br J Dermatol 2006;155:1-8.
5. Pollock PM, Harper UL, Hansen KS, Yudt LM, Stark M, Robbins CM, et al. High frequency of BRAF mutations in nevi. Nat Genet 2003;33:19-20.
6. Bauer J, Curtin JA, Pinkel D, Bastian BC. Congenital melanocytic nevi frequently harbor NRAS mutations but no BRAF mutations. J Invest Dermatol 2007;127:179-82.
7. Stefanaki C, Antoniou C, Stefanaki K, Petrikos G, Argyrakos T, Constantinidou CV, et al. Bcl-2 and Bax in congenital naevi. Br J Dermatol 2006;154:1175-9.
8. Park HJ, Kim BG, Lee SJ, Heo SH, Kim JY, Kwon TH, et al. Proteomic profiling of endothelial cells in human lung cancer. J Proteome Res 2008;7:1138-50.
9. Choi Y-J, Heo S-H, Lee J-M, Cho J-Y. Identification of azurocidin as a potential periodontitis biomarker by a proteomic analysis of gingival crevicular fluid. Proteome Science 2011;9:42.
10. Jensen LJ, Kuhn M, Stark M, Chaffron S, Creevey C, Muller J, et al. STRING 8--a global view on proteins and their functional interactions in 630 organisms. Nucleic Acids Res 2008.
11. Mi H, Dong Q, Muruganujan A, Gaudet P, Lewis S, Thomas PD. PANTHER version 7: improved phylogenetic trees, orthologs and collaboration with the Gene Ontology Consortium. Nucl Acids Res 2010;38:D204-10.
12. Tatusov RL, Fedorova ND, Jackson JD, Jacobs AR, Kiryutin B, Koonin EV, et al. The COG database: an updated version includes eukaryotes. BMC Bioinformatics 2003;4:41.
13. Bindea G, Mlecnik B, Hackl H, Charoentong P, Tosolini M,

Kirilovsky A, et al. ClueGO: a Cytoscape plug-in to decipher functionally grouped gene ontology and pathway annotation networks. Bioinformatics 2009;25:1091-3.
14. Foekens JA, Look MP, Bolt-de Vries J, Meijer-van Gelder ME, van Putten WL, Klijn JG. Cathepsin-D in primary breast cancer: prognostic evaluation involving 2810 patients. Br J Cancer 1999;79:300-7.
15. Losch A, Schindl M, Kohlberger P, Lahodny J, Breitenecker G, Horvat R, et al. Cathepsin D in ovarian cancer: prognostic value and correlation with p53 expression and microvessel density. Gynecol Oncol 2004;92:545-52.
16. Bartenjev I, Rudolf Z, Stabuc B, Vrhovec I, Perkovic T, Kansky A. Cathepsin D expression in early cutaneous malignant melanoma. Int J Dermatol 2000;39:599-602.
17. Podhajcer OL, Bover L, Bravo AI, Ledda MF, Kairiyama C, Calb I, et al. Expression of cathepsin D in primary and metastatic human melanoma and dysplastic nevi. J Invest Dermatol 1995;104:340-4.
18. Marchetti D, McQuillan DJ, Spohn WC, Carson DD, Nicolson GL. Neurotrophin stimulation of human melanoma cell invasion: selected enhancement of heparanase activity and heparanase degradation of specific heparan sulfate subpopulations. Cancer Res 1996;56:2856-63.
19. Marchetti D, Nicolson GL. Human melanoma cell invasion: selected neurotrophin enhancement of invasion and heparanase activity. J Investig Dermatol Symp Proc 1997;2:99-105.
20. Bruning A, Juckstock J, Blankenstein T, Makovitzky J, Kunze S, Mylonas I. The metastasis-associated gene MTA3 is downregulated in advanced endometrioid adenocarcinomas. Histol Histopathol 2010;25:1447-56.
21. Hanahan D, Weinberg RA. The hallmarks of cancer. Cell 2000;100:57-70.
22. Garber K. Energy Boost: The Warburg Effect Returns in a New Theory of Cancer. Journal of the National Cancer Institute 2004;96:1805-6.
23. Bernard K, Litman E, Fitzpatrick JL, Shellman YG, Argast G, Polvinen K, et al. Functional Proteomic Analysis of Melanoma Progression. Cancer Res 2003;63:6716-25.
24. Takahashi Y. The 14-3-3 proteins: gene, gene expression, and function. Neurochem Res 2003;28:1265-73.
25. Datta SR, Katsov A, Hu L, Petros A, Fesik SW, Yaffe MB, et al. 14-3-3 proteins and survival kinases cooperate to inactivate BAD

by BH3 domain phosphorylation. Mol Cell 2000;6:41-51.
26. Tzivion G, Shen YH, Zhu J. 14-3-3 proteins; bringing new definitions to scaffolding. Oncogene 2001;20:6331-8.
27. Tzivion G, Avruch J. 14-3-3 proteins: active cofactors in cellular regulation by serine/threonine phosphorylation. J Biol Chem 2002;277:3061-4.
28. Aprelikova O, Pace AJ, Fang B, Koller BH, Liu ET. BRCA1 is a selective co-activator of 14-3-3 sigma gene transcription in mouse embryonic stem cells. J Biol Chem 2001;276:25647-50.
29. Vakifahmetoglu H, Olsson M, Tamm C, Heidari N, Orrenius S, Zhivotovsky B. DNA damage induces two distinct modes of cell death in ovarian carcinomas. Cell Death Differ 2008;15:555-66.
30. Guweidhi A, Kleeff J, Giese N, El Fitori J, Ketterer K, Giese T, et al. Enhanced expression of 14-3-3sigma in pancreatic cancer and its role in cell cycle regulation and apoptosis. Carcinogenesis 2004;25:1575 - 85.
31. Ito Y, Miyoshi E, Uda E, Yoshida H, Uruno T, Takamura Y, et al. 14-3-3 sigma possibly plays a constitutive role in papillary carcinoma, but not in follicular tumor of the thyroid. Cancer Lett 2003;200:161 - 6.
32. Ferguson A, Evron E, Umbricht C, Pandita T, Chan T, Hermeking H, et al. High frequency of hypermethylation at the 14-3-3sigma locus leads to gene silencing in breast cancer. Proc Natl Acad Sci USA 2000;97:6049 - 54.
33. Hermeking H. The 14-3-3 cancer connection. Nat Rev Cancer 2003;3:931-43.
34. Su TT, Parry DH, Donahoe B, Chien CT, O'Farrell PH, Purdy A. Cell cycle roles for two 14-3-3 proteins during Drosophila development. J Cell Sci 2001;114:3445-54.
35. Toyo-oka K, Shionoya A, Gambello MJ, Cardoso C, Leventer R, Ward HL, et al. 14-3-3epsilon is important for neuronal migration by binding to NUDEL: a molecular explanation for Miller-Dieker syndrome. Nat Genet 2003;34:274-85.
36. Brunet A, Kanai F, Stehn J, Xu J, Sarbassova D, Frangioni JV, et al. 14-3-3 transits to the nucleus and participates in dynamic nucleocytoplasmic transport. J Cell Biol 2002;156:817-28.
37. Zuo S, Xue Y, Tang S, Yao J, Du R, Yang P, et al. 14-3-3 Epsilon Dynamically Interacts with Key Components of Mitogen-Activated Protein Kinase Signal Module for Selective Modulation of the TNF-α-Induced Time Course-Dependent NF-κB Activity. Journal of proteome research 2010;9:3465-78.

38. Liang S, Xu Y, Shen G, Liu Q, Zhao X, Xu Z, et al. Quantitative protein expression profiling of 14-3-3 isoforms in human renal carcinoma shows 14-3-3 epsilon is involved in limitedly increasing renal cell proliferation. Electrophoresis 2009;30:4152-62.
39. Liu Y, Tian RF, Li YM, Liu WP, Cao L, Yang XL, et al. The expression of seven 14-3-3 isoforms in human meningioma. Brain Res 2010;1336:98-102.
40. Che XH, Chen H, Xu ZM, Shang C, Sun KL, Fu WN. 14-3-3epsilon contributes to tumour suppression in laryngeal carcinoma by affecting apoptosis and invasion. BMC Cancer 2010;10:306.
41. Choi K-C, Lee S, Kwak SY, Kim M-S, Choi HK, Kim KH, et al. Increased expression of 14-3-3[var epsilon] protein in intrinsically aged and photoaged human skin in vivo. Mechanisms of Ageing and Development;126:629-36.

APPENDICES

Supplementary Figure 1

Normal 1

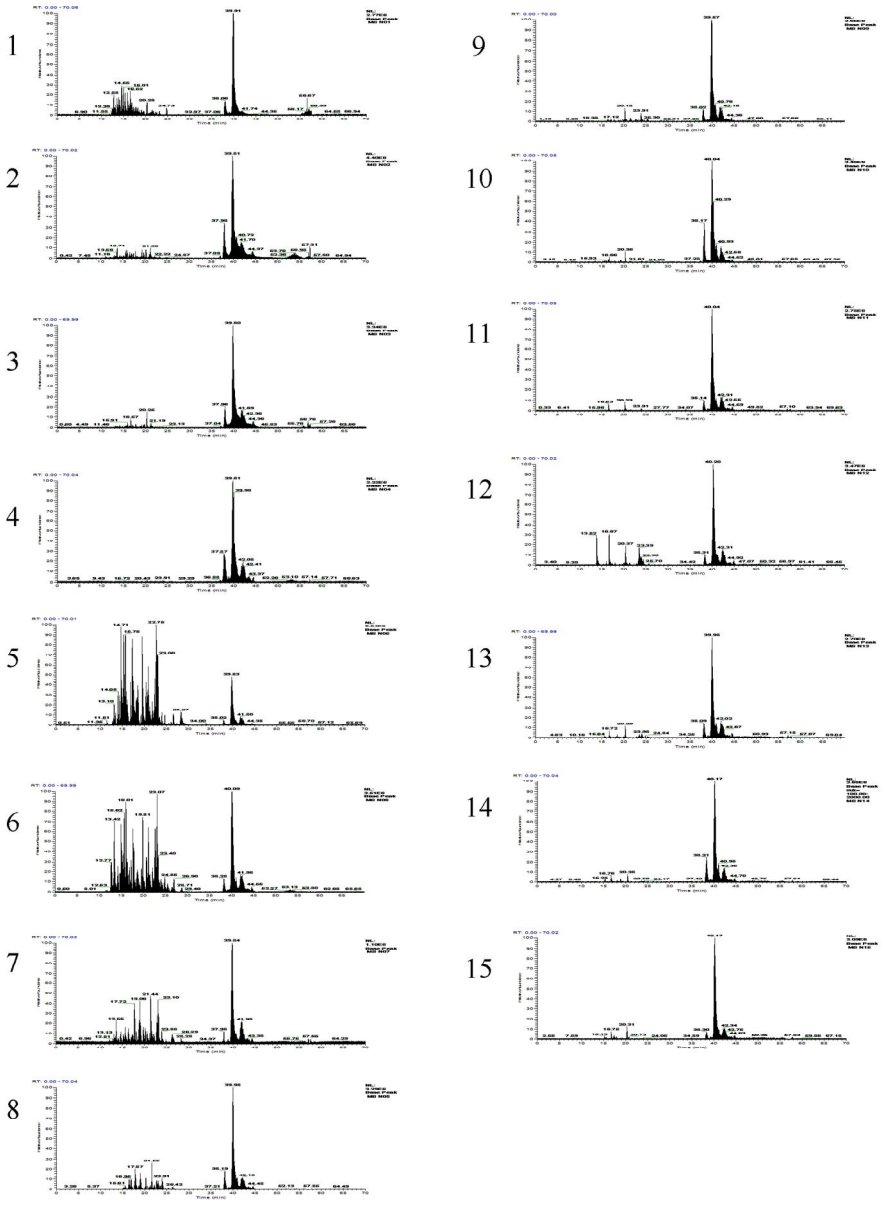

Supplementary Figure 1

Normal 2

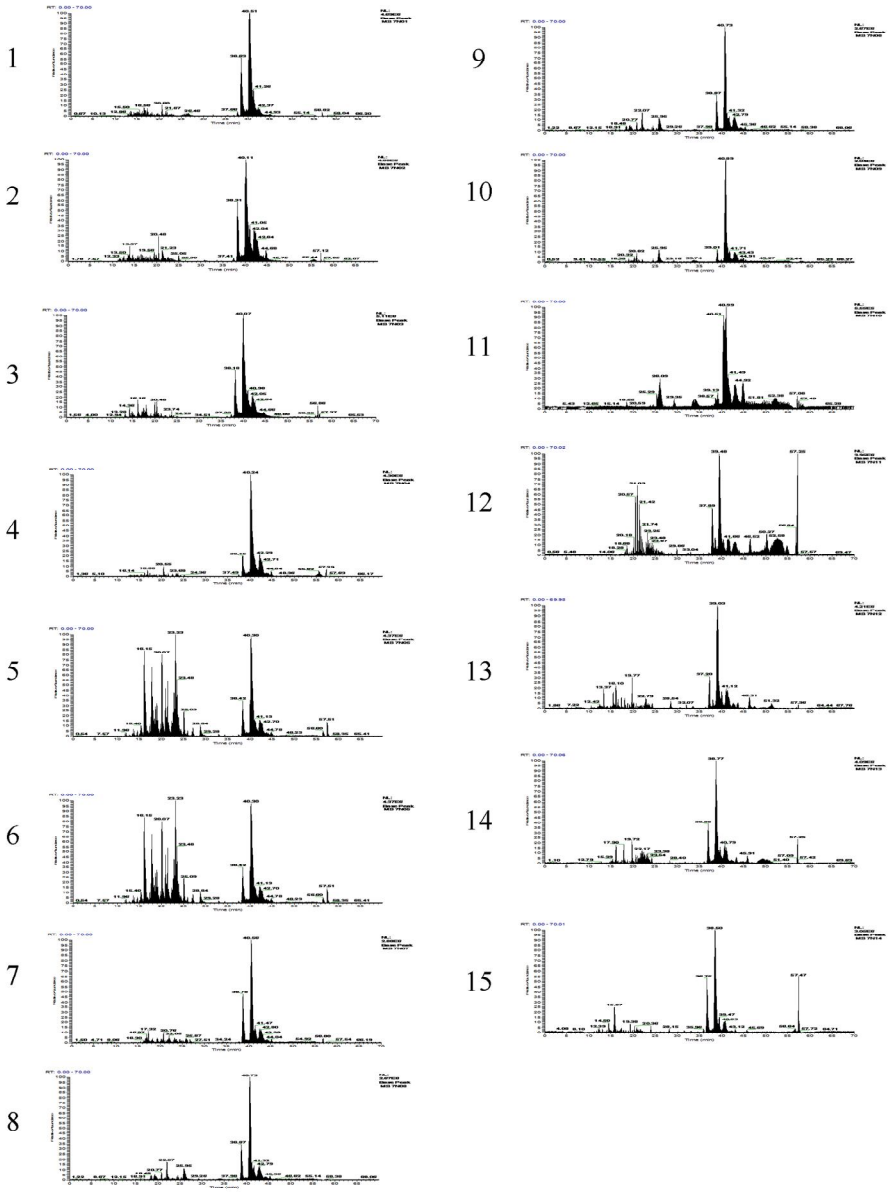

Supplementary Figure 1

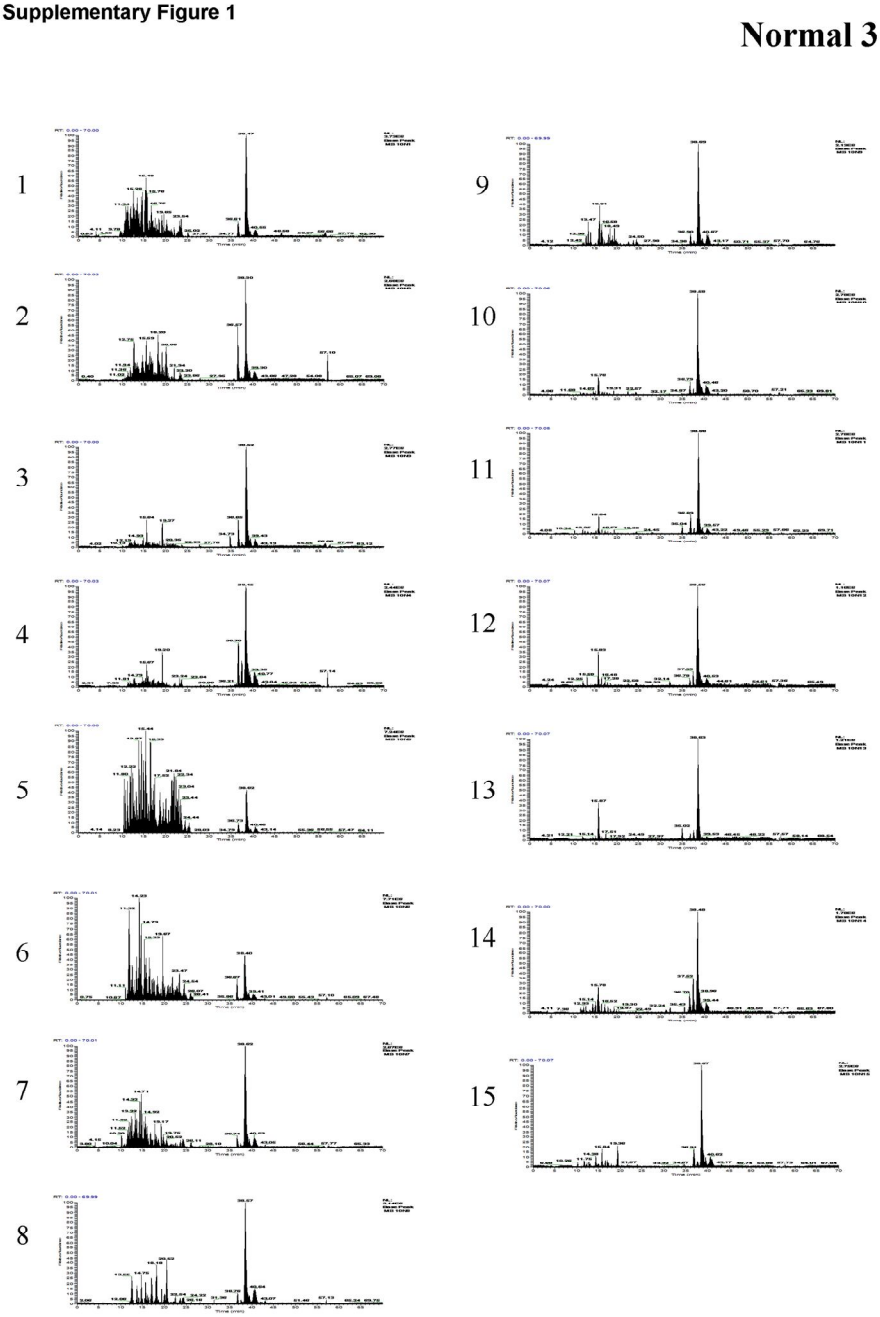

Supplementary Figure 1

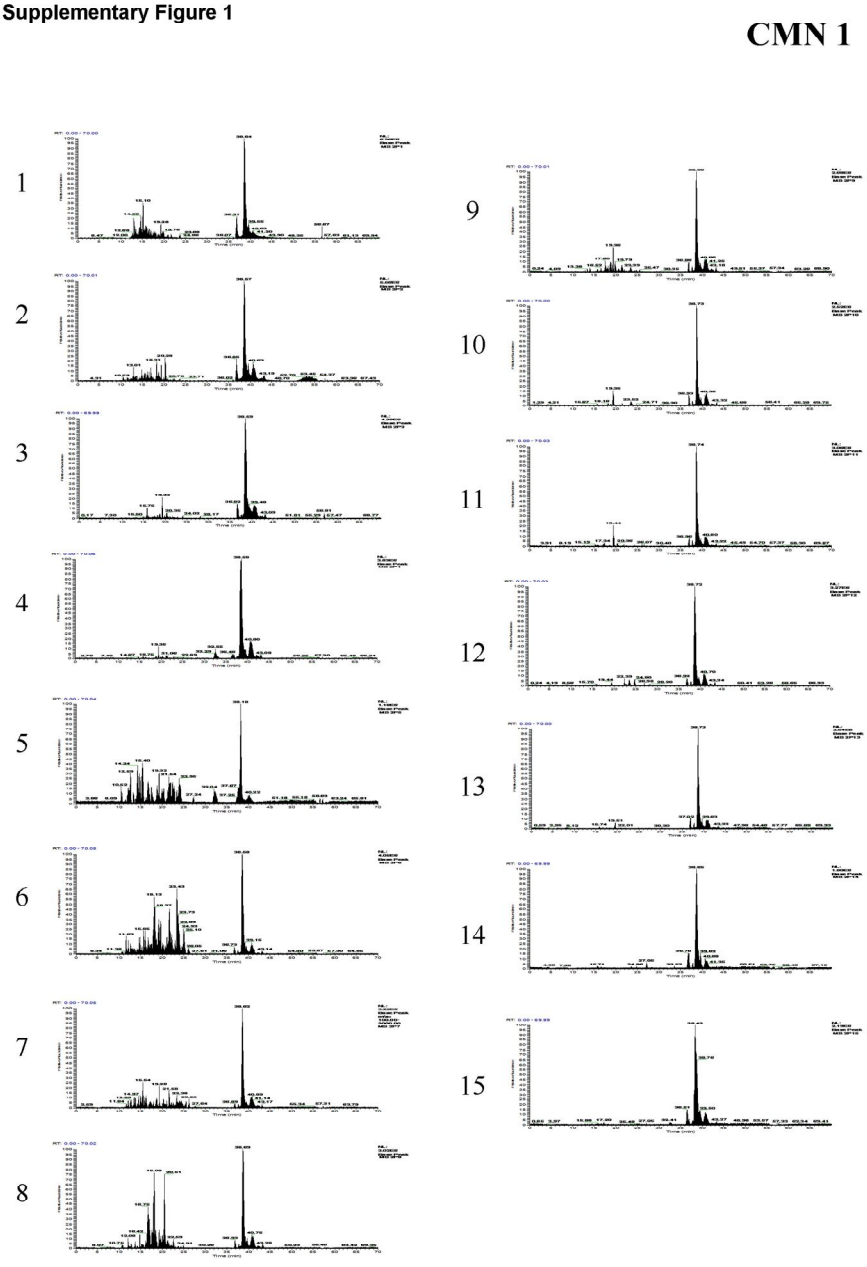

Supplementary Figure 1

CMN 2

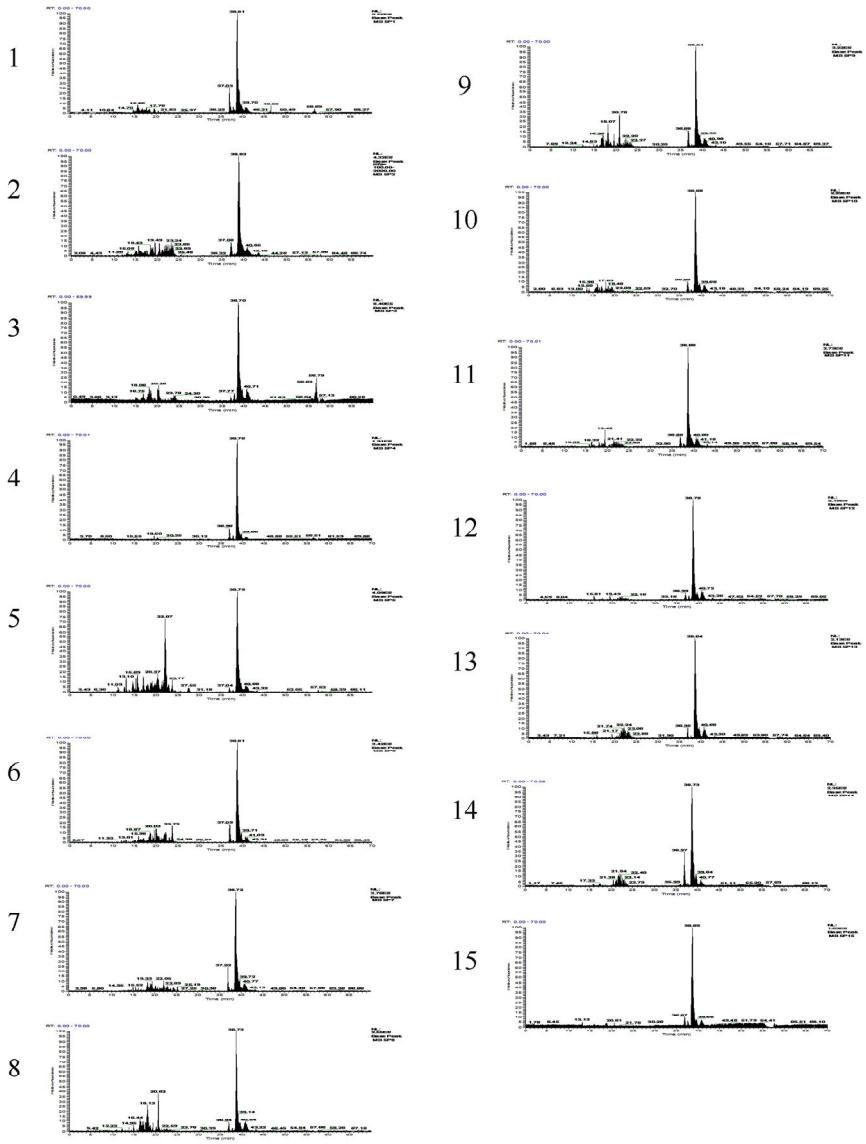

Supplementary Figure 1

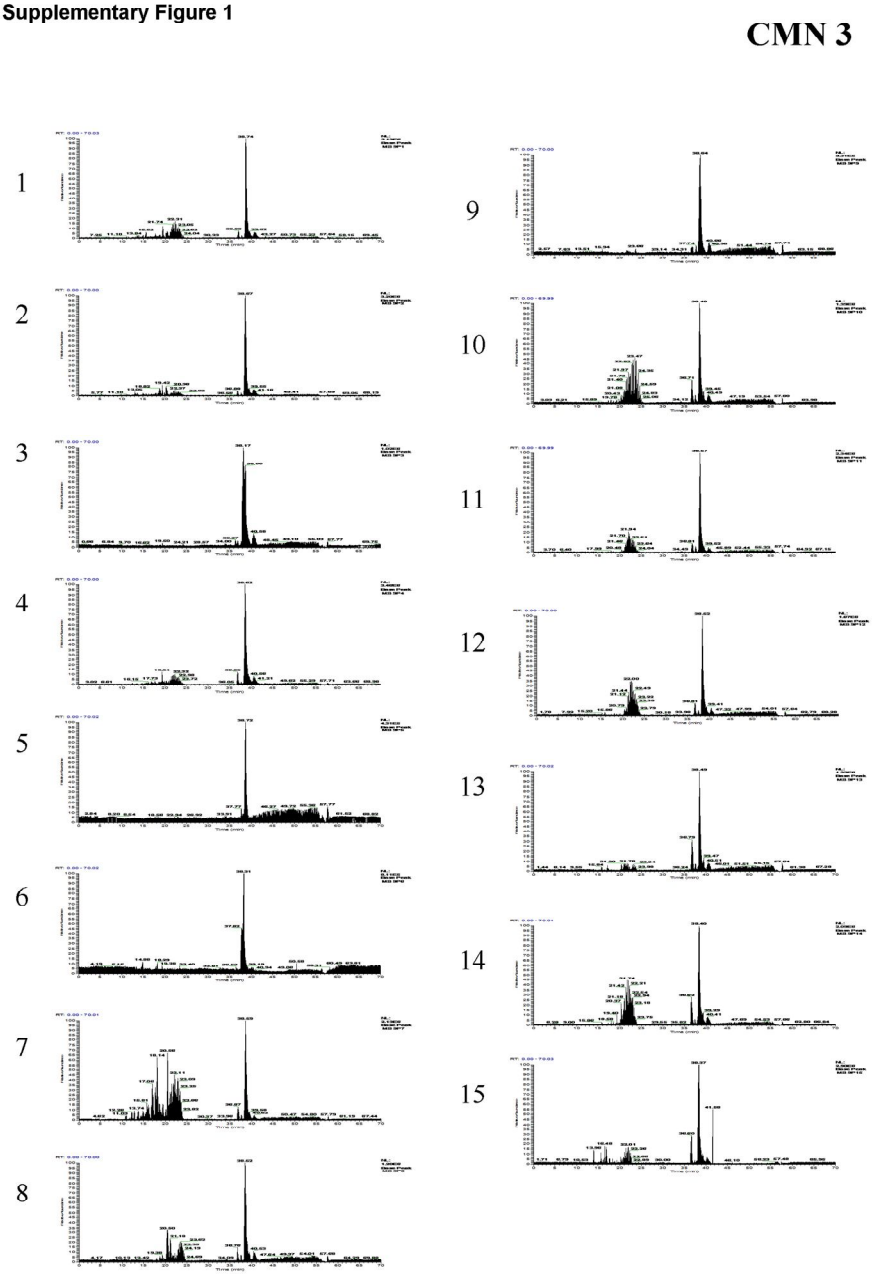

Supplementary Figure S1. Peptide mass peak of 15 bands dissected from a 1D gel of normal skin and GCMN.

Supplementary Figure 2

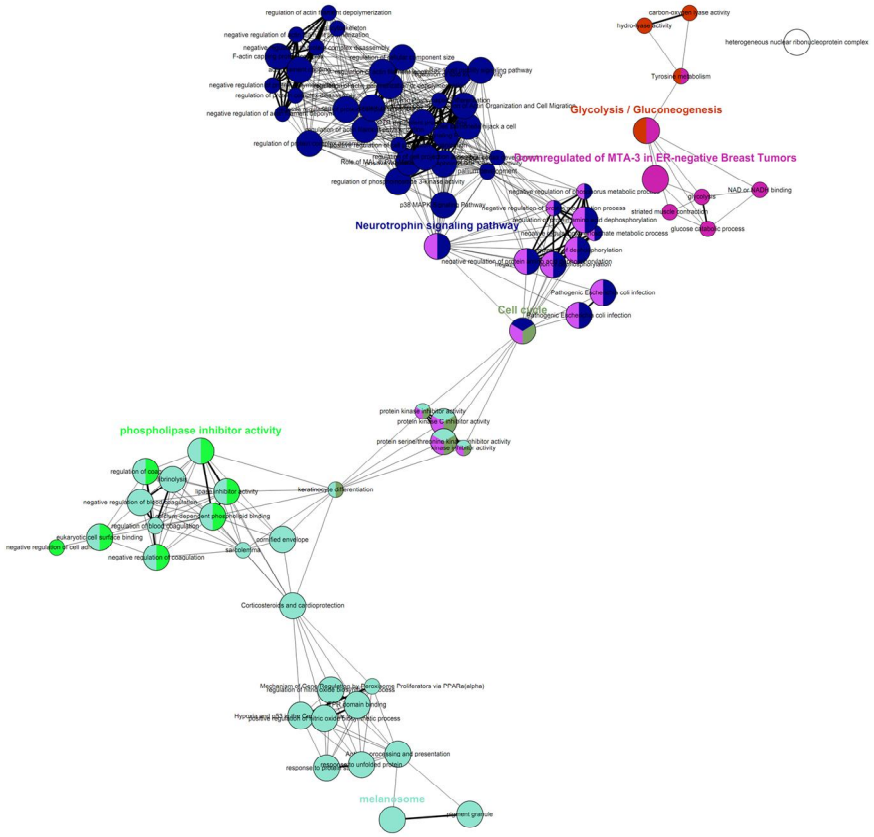

Supplementary Figure S2. The functional network and enriched functional group of GCMN was analyzed using ClueGO, a biological term enrichment analyzer. The following proteins were significantly enriched in GCMN: melanosome (GO_cellular component), neurotrophin signaling pathway (KEGG pathway), downregulated of MTA-3 in ER-negative breast tumors (Biocarta), cell cycle (KEGG pathway), phospholipase inhibitor activity (GO_molecular function), and glycolysis/gluconeogenesis (KEGG pathway).

Supplementary Table 1. Differentially expressed proteins in GCMN

Identified proteins	Accession number[1]	Symbol	p-Value	Fold-change	GeneID[2]
Post-translational modification, protein turnover, chaperones (15)					
CTSD cathepsin D	IPI00011229	CTSD	0.024	6.8	1509
HSP90AA1 heat shock protein 90-kDa alpha (cytosolic), class A member 1 isoform 1	IPI00382470	HSP90AA1	0.02	3.4	3320
HSP90AB1 heat shock protein HSP 90-beta	IPI00414676	HSP90AB1	0.013	3.6	3326
HSPA1A;HSPA1B heat shock 70-kDa protein 1	IPI00304925	HSPA1A	0.031	2.4	3303
HSPA8 Isoform 1 of heat shock cognate 71-kDa protein	IPI00003865	HSPA8	0.0016	5.2	3312
HSPB1 heat shock protein beta-1	IPI00025512	HSPB1	0.0027	3.8	3315
PDIA3 protein disulfide-isomerase A3	IPI00025252	PDIA3	0.012	5.4	2923
PHB prohibitin	IPI00017334	PHB	0.025	5.3	5245
PSMB1 proteasome subunit beta type-1	IPI00025019	PSMB1	0.045	3.5	5689
SFN Isoform 1 of 14-3-3 protein sigma	IPI00013890	SFN	0.027	1.7	2810

YWHAB long isoform of 14-3-3beta/alpha	IPI00216318	YWHAB	0.0012	2.2	7529
YWHAE 14-3-3 epsilon	IPI00000816	YWHAE	0.0051	4.2	7531
YWHAG 14-3-3gamma	IPI00220642	YWHAG	0.024	2.1	7532
YWHAQ 14-3-3theta	IPI00018146	YWHAQ	0.00088	3.3	10971
YWHAZ 14-3-3zeta/delta	IPI00021263	YWHAZ	0.0021	2.6	7534
Cytoskeleton (6)					
A26C1A isoform 1 of ANKRD26-like family C member 1A	IPI00479743	A26C1A	0.0029	4.5	445582
ACTB actin, cytoplasmic 1	IPI00021439	ACTB	0.0027	2.3	60
CAPZA1 F-actin-capping protein subunit alpha-1	IPI00005969	CAPZA1	0.0044	2.6	829
CAPZB cDNA, FLJ93598, highly similar to *Homo sapiens* capping protein (actin filament) muscle Z-line, beta	IPI00641107	CAPZB	0.017	2.9	832
Isoform 2 of dynein heavy chain 2, axonemal	IPI00651691	DNAH2	0.004	2.3	146754
Isoform 2 of myosin light chain kinase, smooth muscle	IPI00221255	MYLK	0.0018	2.6	4638

General function prediction only (5)					
CDC42 Isoform 2 of cell-division control protein 42 homolog	IPI00016786	CDC42	0.017	2.8	998
CSPG4 chondroitin sulfate proteoglycan 4	IPI00019157	CSPG4	0.026	2.3	1464
HNRNPA2B1 isoform B1 of heterogeneous nuclear ribonucleoproteins A2/B1	IPI00396378	HNRNPA2B1	0.015	4.9	3181
PEBP1 phosphatidylethanolamine-binding protein 1	IPI00219446	PEBP1	0.026	2.9	5037
RAC1 isoform A of Ras-related C3 botulinum toxin substrate 1	IPI00010271	RAC1	0.0092	3.7	5879
Carbohydrate transport and metabolism (4)					
ALDOA fructose-bisphosphate aldolase A	IPI00465439	ALDOA	0.034	4.0	226
Uncharacterized protein ENSP00000348237	IPI00453476		0.0012	3.1	
FLG2 filaggrin-2	IPI00397801	FLG2	0.000021	0.2	388698
GAPDH glyceraldehyde 3-phosphate dehydrogenase	IPI00219018	GAPDH	0.035	2.2	2597
Energy production and conversion (3)					
ATP5B ATP synthase subunit beta, mitochondrial	IPI00303476	ATP5B	0.032	5.0	506

ETFA electron transfer flavoprotein subunit alpha, mitochondrial	IPI00010810	ETFA	0.0028	3.4	2108
NDUFS3 NADH dehydrogenase [ubiquinone] iron-sulfur protein 3, mitochondrial	IPI00025796	NDUFS3	0.03	1.7	4722
Signal transduction mechanisms (3)					
ARHGDIA rho GDP-dissociation inhibitor 1	IPI00003815	ARHGDIA	0.047	3.4	396
FBLN5 fibulin-5	IPI00294615	FBLN5	0.0028	3.4	10516
RYR3 uncharacterized protein RYR3	IPI00217185	RYR3	0.013	2.7	6263
Intracellular trafficking, secretion, and vesicular transport (3)					
ANXA1 annexin A1	IPI00218918	ANXA1	0.03	3.0	301
ANXA2 annexin A2 isoform 1	IPI00418169	ANXA2	0.0059	1.8	302
ANXA5 annexin A5	IPI00329801	ANXA5	0.025	3.8	308
Amino acid transport and metabolism (2)					
PHGDH D-3-phosphoglycerate dehydrogenase	IPI00011200	PHGDH	0.031	5.0	26227
TPSB2 TPSB2	IPI00419942	TPSB2	0.043	2.2	64499

Lipid transport and metabolism (2)					
ECH1 delta(3,5)-delta(2,4)-dienoyl-CoA isomerase, mitochondrial	IPI00011416	ECH1	0.00034	3.1	1891
FASN fatty acid synthase	IPI00026781	FASN	0.023	3.1	2194
Translation, ribosomal structure, and biogenesis (2)					
EEF1A1 elongation factor 1-alpha 1	IPI00396485	EEF1A1	0.012	2.5	1915
RPSA 33-kDa protein	IPI00413108	RPSA	0.024	2.9	3921
RNA processing and modification (1)					
HNRNPU short isoform of heterogeneous nuclear ribonucleoprotein U	IPI00479217	HNRNPU	0.0037	2.3	3192
Cell cycle control, cell division, chromosome partitioning (1)					
KRT1 keratin, type II cytoskeletal 1	IPI00220327	KRT1	0.016	0.7	3848
Inorganic ion transport and metabolism (1)					
CLIC1 chloride intracellular channel protein 1	IPI00010896	CLIC1	0.015	3.5	1192
Secondary metabolites biosynthesis, transport, and catabolism (1)					
ADH1B alcohol dehydrogenase 1B	IPI00473031	ADH1B	0.025	0.2	125

Function unknown (1)					
HRNR hornerin	IPI00398625	HRNR	0.035	0.2	388697

Accession Number[1]: International Protein Index (IPI) accession number, GeneID[2]: NCBI GeneID

ABSTRACT IN KOREAN

선천성 거대 멜라닌 모반증의 단백질체 분석

<지도교수 탁 관 철 >

연세대학교 대학원 의학과

김 용 규

연구배경: 선천성 거대 멜라닌 모반증은 임상적인 측면에서 두 가지 중요한 면이 있다. 첫째로는 미용적으로 외모가 손상되어 환자와 부모에게 정신적 경제적으로 어려운 문제가 되며 둘째로 흑색종으로의 발병확률이 있다는 것이다. 그러나 선천성 거대 멜라닌 모반증의 발생원인이나 흑색종이 발병되는 기전에 대한 단백질체 수준의 연구는 알려져 있지 않다.

연구목적: 본 연구의 목적은 선천성 거대 멜라닌 모반증에서 야기되는 단백질체의 변화양상을 파악 하고, 단백질체의 변화에 의해 야기 될 수 있는 기능적 변화를 분석하여, 선천성 거대 모반증의 분자 수준의 이해와 흑색종발병과의 상관관계를 규명하고자 한다.

연구방법: 6명의 선천성 거대 모반증 환아에서 6개의 선천성 거대 모반 조직과 3개의 정상 피부 조직을 채취하였으며 정상 환아에서 3개의 피부 조직을 채취하였다. 각각 3개씩의 정상 피부조직과 선천성 멜라닌 모반증 피부조직의 단백질체 분석을 액상 크로마토그래픽 텐덤 질량분석법 (LC-MS/MS 분석)으로 분석 비교하였으며, 의미있는 단백질의 상대적 발현 변화를 각각 3개씩의 정상과 선천성 멜라닌 모반증 조직에서 Western blot 분석을 통해 확인하였다. 정상과 질병군에 발현 변화가 유의하게 변화되는 단백질들을 선별하여, 이들 단백질군의 시스템적 분석을 생체정보학 분석 프로그램들을 이용하여 분석하였다.

연구결과: 정상과 질병군의 피부 단백질체 분석에서 50개 단백질이 발현량에 유의한 차이를 보였으며 ($p<0.05$). 질병군에서 4개의 단백질 발현량이 감소하였으며, 46개 단백질의 발현량이 증가하였다. 발현 변화단백질들은 분자적 기능 분석 상에서 샤페론 단백질(chaperone proteins)이 15.7% 로 가장 높은 비율을 차지하였으며, 생물학적 기능분석 상에서는 신호 전달 단백질이 15.3%로 가장 높은 비율로

분석되었다. 특히 질병군의 단백질 변화는 뉴트로핀 신호조절, 멜라노좀, 에스트로겐 수용체 음성(ER-negative) 유방암 관련 단백질군등과 기능적 연관을 가지고 있었다. 또한, 질병군에서 14-3-3 단백질군의 발현이 질병군에서 크게 증가하였으며. Western blot 분석 결과, 14-3-3 엡실론 발현 증가가 확인 되었다.

결론: 선천성 멜라닌 모반증의 단백질체 분석을 통해 14-3-3 단백질들의 증가를 확인하였으며 이것이 선천성 거대 모반증의 생물학적 경로 리모델링의 중요한 단백질일 가능성이 있음을 발견하였다. 특히 14-3-3 엡실론의 증가는 발생학적으로 선천성 멜라닌 모반증의 발현과 밀접한 관련이 있으며 흑색종의 발병과도 연관성이 있을 것으로 추정되며 선천성 거대 모반증 환자에서 흑생종으로 발현된 환자와의 비교에 대한 추가 연구가 필요하다

핵심 되는 말: 선천성 멜라닌 모반증, 흑색종, 14-3-3 엡실론